INTERNATIONAL JOURNAL FOR NUMERICAL METHODS IN ENGINEERING
Int. J. Numer. Meth. Engng. **46**, 1575–1591 (1999)

THERMO-MECHANICAL ANALYSIS OF INDUSTRIAL SOLIDIFICATION PROCESSES

MIGUEL CERVERA*, CARLOS AGELET DE SARACIBAR AND MICHELE CHIUMENTI

International Center for Numerical Methods in Engineering (*CIMNE*), *Universidad Politécnica de Cataluña*, *Campus Norte UPC*, *08034 Barcelona*, *Spain*

SUMMARY

The paper presents an up-to-date finite element numerical model for fully coupled thermo-mechanical problems, focussing in the simulation of solidification processes of industrial metal parts. The proposed constitutive model is defined by a thermo-visco-elasto-(visco)plastic free energy function which includes a contribution for thermal multiphase changes. Mechanical and thermal properties are assumed to be temperature-dependent, and viscous-like strains are introduced to account for the variation of the elastic moduli during the cooling process. The continuous transition between the initial fluid-like and the final solid-like behaviour of the part is modelled by considering separate viscous and elasto-plastic responses as a function of the solid fraction. Thermo-mechanical contact conditions between the mould and the part are specifically considered, assuming that the heat flux is a function of the normal pressure and the thermal and mechanical gaps. A fractional step method arising from an operator split of the governing equations is used to solve the non-linear coupled system of equations, leading to a staggered product formula solution algorithm suitable for large-scale computations. Representative simulations of industrial solidification processes are shown, and comparison of computed results using the proposed model with available experimental data is given. Copyright © 1999 John Wiley & Sons, Ltd.

KEY WORDS: thermo-mechanical analysis; solidification processes; coupled solution

1. INTRODUCTION

The numerical simulation of coupled thermo-mechanical solidification processes has been one of the research topics of great interest over the last years. Also, during the last decade, a growing interest on this and related topics has been shown by many industrial companies, such as automotive and aeronautical, motivated by the need to get high-quality final products and to reduce manufacturing costs. However, and despite the enormous progress achieved lately in computational mechanics, the large-scale numerical simulation of these problems continues to be nowadays a very complex task. This is mainly due to the highly non-linear nature of the problem, usually involving non-linear constitutive behaviour, liquid–solid and solid–solid phase changes, non-linear

* Correspondence to: Miguel Cervera, ETS Ingenieros de Caminos, CyP, Universidad Politécnica de Cataluña, Campus Norte UPC-Modulo C1, Gran Capitan s/n, 08034 Barcelona, Spain. E-mail: cervera@cimne.upc.es

Contract/grant sponsor: Renault; contract/grant number: CIMNE/1997/001

CCC 0029-5981/99/331575–17$17.50

Received 1 September 1998
Revised 1 February 1999

thermal and mechanical boundary conditions, frictional contact interaction and complex coupled thermo-mechanical phenomena. In this paper the topic of the numerical simulation of industrial solidification processes is addressed.

2. FORMULATION OF THE THERMO-MECHANICAL PROBLEM

2.1. Local governing equations

The local system of partial differential equations governing the (quasi-static) coupled thermo-mechanical initial boundary value problem is defined by the momentum and energy balance equations, restricted by the inequalities arising from the second law of the thermodynamics. The local form of the momentum and energy balance equations can be written as

$$\begin{aligned} 0 &= \nabla \cdot \boldsymbol{\sigma} + \mathbf{B} \\ \boldsymbol{\Theta}\, \dot{S} &= -\nabla \cdot \mathbf{q} + R + \mathscr{D}_{\text{int}} \end{aligned} \tag{1}$$

where $\mathbf{B}$ are the (prescribed) body forces, $\nabla \cdot (\cdot)$ the divergence operator, $\boldsymbol{\sigma}$ the Cauchy stress tensor, Θ the absolute temperature, S the entropy, $\mathbf{q}$ the heat flux, R the (prescribed) heat source and $\mathscr{D}_{\text{int}}$ the internal dissipation per unit volume. Additionally, suitable prescribed boundary and initial conditions must be supplied, as well as considering the equilibrium equations at the contact interfaces.

Also, the entropy S and the Cauchy stress tensor $\boldsymbol{\sigma}$ must be defined via constitutive relations, subjected to the following restriction on the internal dissipation [1]:

$$\mathscr{D}_{\text{int}} = \boldsymbol{\sigma} : \dot{\boldsymbol{\varepsilon}} + \Theta \dot{S} - \dot{E} \geqslant 0 \tag{2}$$

where $\boldsymbol{\varepsilon}$ is the infinitesimal strain tensor and E is the internal energy. The heat flux $\mathbf{q}$ is related to the absolute temperature through Fourier's law ($\mathbf{q} = -k(\Theta)\nabla\Theta$, with $k = k(\Theta)$ being the temperature-dependent thermal conductivity), subjected to the restriction on the dissipation by conduction

$$\mathscr{D}_{\text{con}} = -\frac{1}{\Theta}\nabla\Theta \cdot \mathbf{q} = \frac{k(\Theta)}{\Theta}\nabla\Theta \cdot \nabla\Theta \geqslant 0 \tag{3}$$

2.2. Thermo-mechanical constitutive model for the solid phase

In order to define a thermo-(visco)elastic-(visco)plastic constitutive model for the solid phase let us introduce the free energy ($\Psi = E - \Theta S$), with the functional form

$$\Psi = \hat{\Psi}(\boldsymbol{\varepsilon}, \boldsymbol{\varepsilon}_{\text{v}}, \boldsymbol{\varepsilon}_{\text{p}}, \xi, \Theta) = \hat{W}(\boldsymbol{\varepsilon}, \boldsymbol{\varepsilon}_{\text{v}}, \boldsymbol{\varepsilon}_{\text{p}}, \Theta) + \hat{H}(\xi, \Theta) + \hat{T}(\Theta) \tag{4}$$

In this expression $W = \hat{W}(\boldsymbol{\varepsilon}, \boldsymbol{\varepsilon}_{\text{v}}, \boldsymbol{\varepsilon}_{\text{p}}, \Theta)$ is the mechanical contribution, $H = \hat{H}(\xi, \Theta)$ is the plastic hardening potential and $T = \hat{T}(\Theta)$ is the thermal contribution. The internal variables of the model are: the viscous strain tensor $\boldsymbol{\varepsilon}_{\text{v}}$, the plastic strain tensor $\boldsymbol{\varepsilon}_{\text{p}}$, and the equivalent plastic strain ξ. Let us define the elastic strain tensor $\boldsymbol{\varepsilon}_{\text{e}}$, as

$$\boldsymbol{\varepsilon}_{\text{e}} = \boldsymbol{\varepsilon} - \boldsymbol{\varepsilon}_{\text{v}} - \boldsymbol{\varepsilon}_{\text{p}} - \boldsymbol{\varepsilon}_{\Theta} \tag{5}$$

where the thermal strain tensor is defined as

$$\boldsymbol{\varepsilon}_\Theta = \tfrac{1}{3}\, e_\Theta\, \mathbf{1} = [\alpha(\Theta)(\Theta - \Theta_{\text{ref}}) - \alpha(\Theta_0)(\Theta_0 - \Theta_{\text{ref}})]\mathbf{1} \tag{6}$$

where $e_\Theta = \boldsymbol{\varepsilon}_\Theta : \mathbf{1}$ is the volumetric thermal strain, $\alpha = \alpha(\Theta)$ is the (temperature-dependent) thermal expansion coefficient, Θ_0 is the initial temperature, Θ_{ref} is the reference temperature for the experimental determination of α, and $\mathbf{1}$ is the (second order) unit tensor.

With these definitions, the mechanical part of the free energy can be expressed as

$$W = \hat{W}(\boldsymbol{\varepsilon}, \boldsymbol{\varepsilon}_{\text{v}}, \boldsymbol{\varepsilon}_{\text{p}}, \Theta) = \hat{\bar{W}}(\boldsymbol{\varepsilon}_{\text{e}}, \Theta) = \tfrac{1}{2}\, K(\Theta)\,(e_{\text{e}}^2 - e_\Theta^2) + G(\Theta)\,\text{dev}^2\,[\boldsymbol{\varepsilon}_{\text{e}}] \tag{7}$$

where $K = K(\Theta)$ is the (temperature-dependent) bulk modulus, $G = G(\Theta)$ is the (temperature-dependent) shear modulus, $e_{\text{e}} = \boldsymbol{\varepsilon}_{\text{e}} : \mathbf{1}$ is the elastic volumetric strain and dev$[\,\cdot\,]$ means deviatoric part.

The hardening part of the free energy can be expressed as [2]

$$H = \hat{H}(\xi, \Theta) = \tfrac{1}{2}\, h(\Theta)\, \xi^2 + (y_0(\Theta) - y_\infty(\Theta))[\, \xi - (\, 1 - \exp(-\delta(\Theta)\xi)\,)/\delta(\Theta)] \tag{8}$$

where the linear hardening coefficient $h = h(\Theta)$, the flow stress $y_0 = y_0(\Theta)$, the saturation hardening limit value $y_\infty = y_\infty(\Theta)$, and the saturation hardening exponent $\delta = \delta(\Theta)$, are (temperature-dependent) material properties defining the hardening law.

The thermal term of the free energy can be expressed as [2]

$$T = \hat{T}(\Theta) = \int_{\Theta_0}^{\Theta} \hat{T}_\Theta(\bar{\Theta})\, \mathrm{d}\bar{\Theta} = -\int_{\Theta_0}^{\Theta} \mathrm{d}\bar{\Theta} \int_{\Theta_0}^{\bar{\Theta}} C_0(\hat{\Theta})\, \frac{\mathrm{d}\hat{\Theta}}{\hat{\Theta}} \tag{9}$$

where $C_0 = C_0(\Theta)$ is the (temperature-dependent) heat capacity of the material at constant deformation.

The state equations are obtained from equation (4) using Coleman's method as [1]

$$\begin{aligned} \boldsymbol{\sigma} &= \partial_{\boldsymbol{\varepsilon}} \hat{\Psi} = K(\Theta)\, e_{\text{e}}\, \mathbf{1} + 2\, G(\Theta)\, \text{dev}[\boldsymbol{\varepsilon}_{\text{e}}] \\ S &= -\partial_\Theta \hat{\Psi} = \int_{\Theta_0}^{\Theta} C_0(\hat{\Theta})\, \frac{\mathrm{d}\hat{\Theta}}{\hat{\Theta}} - \partial_\Theta \hat{W} - \partial_\Theta \hat{H} \end{aligned} \tag{10}$$

where the term $-\partial_\Theta \hat{W} = 3K(e_{\text{e}} + e_\Theta)[\alpha + \alpha_\Theta(\Theta_0 - \Theta_{\text{ref}})] - \tfrac{1}{2} K_\Theta(e_{\text{e}}^2 - e_\Theta^2)$ may be different from zero even if the material properties are constant.

The internal dissipation can be expressed in terms of the evolution of the internal variables as

$$\mathscr{D}_{\text{int}} = \boldsymbol{\sigma} : \dot{\boldsymbol{\varepsilon}}_{\text{v}} + \boldsymbol{\sigma} : \dot{\boldsymbol{\varepsilon}}_{\text{p}} + q\, \dot{\xi} \geqslant 0 \tag{11}$$

where q is the conjugate variable of ξ, that is, $q = -\partial_\xi \hat{\Psi} = -\partial_\xi \hat{H}$.

Note that considering the constitutive equation for the entropy and taking its time derivative and applying the chain rule the heat capacity and the elastoplastic heating can be defined as

$$\begin{aligned} C_{\text{s}}(\Theta) &:= \Theta\, \partial_\Theta S = C_0(\Theta) - \Theta\, \partial^2_{\Theta\Theta}\, (\hat{W} + \hat{H}) \\ \mathscr{H}_{\text{ep}}(\Theta) &:= \Theta\, (\partial_{\boldsymbol{\varepsilon}} S : (\dot{\boldsymbol{\varepsilon}}_{\text{e}} + \dot{\boldsymbol{\varepsilon}}_\Theta) + \partial_\xi S\, \dot{\xi}) = -\Theta\, \partial_\Theta\, (\boldsymbol{\sigma} : (\dot{\boldsymbol{\varepsilon}}_{\text{e}} + \dot{\boldsymbol{\varepsilon}}_\Theta) - q\dot{\xi}) \end{aligned} \tag{12}$$

where equation (5) and the equalities $\partial_{\boldsymbol{\varepsilon}} S = -\partial_\Theta \boldsymbol{\sigma}$ and $\partial_\xi S = \partial_\Theta q$ have been used. With these definitions at hand, equation (1.b) can be rewritten in the usual temperature form as

$$C_{\text{s}}\, \dot{\Theta} = -\nabla \cdot \mathbf{q} + R + \mathscr{D}_{\text{int}} - \mathscr{H}_{\text{ep}} \tag{13}$$

In the case of an increase of the temperature-dependent elastic moduli due to the cooling process of a loaded elastic solid, irrecoverable strains necessarily occur. These strains are evident if a sample loaded with given elastic moduli is unloaded at a later time when the temperature has dropped and, therefore, the elastic moduli are higher. This stiffening effect is incorporated in the constitutive model introducing a viscous strain tensor as an internal variable. Taking the time derivative of equation (10a) yields

$$\dot{\boldsymbol{\sigma}} = (K(\Theta)\,\dot{\mathrm{e}}_{\mathrm{e}} + \dot{K}(\Theta)\,e_{\mathrm{e}})\,\mathbf{1} + 2\,G(\Theta)\,\mathrm{dev}[\dot{\boldsymbol{\varepsilon}}_{\mathrm{e}}] + 2\,\dot{G}(\Theta)\,\mathrm{dev}[\boldsymbol{\varepsilon}_{\mathrm{e}}] \tag{14}$$

On the other hand, the experimental observation of the relation between the rate of stress and the rate of strain takes the form

$$\begin{aligned} \dot{\boldsymbol{\sigma}} &= K(\Theta)\,(\dot{\mathrm{e}} - \dot{\mathrm{e}}_{\Theta})\,\mathbf{1} + 2\,G(\Theta)\,\mathrm{dev}[\,\dot{\boldsymbol{\varepsilon}} - \dot{\boldsymbol{\varepsilon}}_{\mathrm{p}}\,] \\ &= K(\Theta)\,(\dot{\mathrm{e}}_{\mathrm{e}} + \dot{\mathrm{e}}_{\mathrm{v}})\,\mathbf{1} + 2\,G(\Theta)\,\mathrm{dev}[\,\dot{\boldsymbol{\varepsilon}}_{\mathrm{e}} + \dot{\boldsymbol{\varepsilon}}_{\mathrm{v}}\,] \end{aligned} \tag{15}$$

Equating equation (14) to equation (15a) yields the following evolution law for the viscous strain:

$$\dot{\boldsymbol{\varepsilon}}_{\mathrm{v}} := \frac{\langle \dot{K} \rangle}{K}\,\mathrm{e}_{\mathrm{e}}\,\mathbf{1} + \frac{\langle \dot{G} \rangle}{G}\,\mathrm{dev}[\boldsymbol{\varepsilon}_{\mathrm{e}}] = \frac{\langle \dot{K} \rangle}{K^2}\,p\,\mathbf{1} + \frac{\langle \dot{G} \rangle}{2G^2}\,\mathrm{dev}[\boldsymbol{\sigma}] \tag{16}$$

where $p = (1/3)\,\boldsymbol{\sigma} : \mathbf{1}$ is the pressure, and the symbols $\langle \cdot \rangle$ are the Macaulay brackets (thus giving the value of the enclosed expression when positive, and setting a zero value if negative). They have been introduced to ensure that the irrecoverable strains only change if the elastic modulus is increasing, this being a thermodynamical requirement to ensure positiveness of the internal dissipation.

Finally, the evolution of the plastic strains is defined in the usual way for a J2-thermo-(visco)-plastic model. Assuming a plastic yield function of the form $\Phi = \hat{\Phi}(\boldsymbol{\sigma}, q, \Theta)$, the evolution laws of the internal variables take the form

$$\dot{\boldsymbol{\varepsilon}}_{\mathrm{p}} := \gamma \partial_{\boldsymbol{\sigma}} \hat{\Phi}(\boldsymbol{\sigma}, q, \Theta) \quad \text{and} \quad \dot{\xi} := \gamma\ \partial_q \hat{\Phi}(\boldsymbol{\sigma}, q, \Theta) \tag{17}$$

where γ is the plastic multiplier. For an inviscid plastic model γ must satisfy the Kuhn–Tucker ($\gamma \geqslant 0, \Phi \leqslant 0, \gamma\Phi = 0$) and consistency ($\gamma\dot{\Phi} = 0$) conditions. If a Perzyna-type visco-plastic model is used, γ is given by

$$\gamma = \frac{1}{\eta_{\mathrm{p}}(\Theta)} \langle \hat{\Phi}(\boldsymbol{\sigma}, q, \Theta) \rangle \geqslant 0 \tag{18}$$

where $\eta_{\mathrm{p}} = \eta_{\mathrm{p}}(\Theta) \geqslant 0$ is the (temperature-dependent) plastic viscosity of the material.

In this work, the Von Mises yield criterion is used, so that

$$\hat{\Phi}(\boldsymbol{\sigma}, q, \Theta) = \mathrm{dev}^2\,[\boldsymbol{\sigma}] - \sqrt{\tfrac{2}{3}}\,[y_0(\Theta) - q] = \mathrm{dev}^2\,[\boldsymbol{\sigma}] - \sqrt{\tfrac{2}{3}}\,\sigma_Y \leqslant 0 \tag{19}$$

Note that the Macaulay brackets introduced in equation (16) for the evolution law of the viscous strains, plus the associative character of evolution law of the plastic internal variables, ensure the positiveness of the internal dissipation (see equation (11)).

2.3. Thermo-mechanical constitutive model with phase change

The constitutive model presented above for the solid phase will now be extended to account for the phase change phenomena. The principles of this extension are twofold: (a) to include the

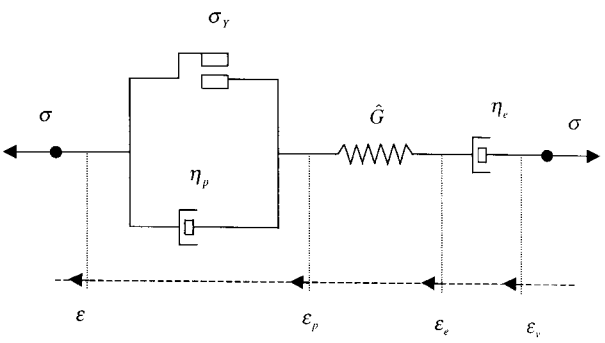

Figure 1. Rheological mechanical model with phase change

stress behaviour in the liquid phase and during the phase change, and (b) to include the thermal effects due to the phase change.

To comply with the first principle, it is assumed that the liquid phase behaves as a (degenerated) visco-elastic material, according to Norton's model [3]. During the phase change, a continuous transition between the liquid-phase and the solid-phase behaviour is constructed by considering that both phases work in a series arrangement, as a visco-elastic-visco-plastic Maxwell element (see Figure 1).

Let us define the solid and liquid fractions as functions of the temperature, $f_s = f_s(\Theta)$ and $f_l = f_l(\Theta) = 1 - f_s(\Theta)$, respectively ($f_s(\Theta) = 0$ for $\Theta \geqslant \Theta_l$ and $f_s(\Theta) = 1$ for $\Theta \leqslant \Theta_s$, Θ_l and Θ_s being the *liquidus* and *solidus* temperatures, respectively). Equation (7) is now rewritten as

$$W = \hat{W}(\boldsymbol{\varepsilon}, \boldsymbol{\varepsilon}_v, \boldsymbol{\varepsilon}_p, \Theta) = \hat{W}(\boldsymbol{\varepsilon}_e, \Theta) = \tfrac{1}{2} K(\Theta)(e_e^2 - e_\Theta^2) + \hat{G}(\Theta)\,\mathrm{dev}^2[\boldsymbol{\varepsilon}_e] \tag{20}$$

where $\hat{G} = G(\Theta)/f_s(\Theta)$ is the effective (temperature-dependent) shear modulus. The evolution law of the viscous strains, equation (16), is also modified to account for the viscous behaviour of the fluid, and it is rewritten as

$$\dot{\boldsymbol{\varepsilon}}_v := \frac{\langle \dot{K} \rangle}{K^2}\, p\,\mathbf{1} + \left(\frac{\langle \dot{\hat{G}} \rangle}{2\hat{G}^2} + \frac{1}{\hat{\eta}_e} \right) \mathrm{dev}[\boldsymbol{\sigma}] \tag{21}$$

where the $\hat{\eta}_e = \eta_e(\Theta)/f_l(\Theta)$ is the effective (temperature-dependent) elastic viscosity. Note that for the solid phase $f_l(\Theta) = 0$ and, therefore, $\hat{\eta}_e = \infty$, and the solid model is recovered. On the other hand, for the fluid phase $f_s(\Theta) = 0$ and, therefore, $\hat{G} = \infty$ and a pure Norton's model is recovered.

Also the volumetric change due to the phase change is included, so that equation (6) is rewritten as

$$\boldsymbol{\varepsilon}_\Theta = [\alpha(\Theta)(\Theta - \Theta_{\mathrm{ref}}) - \alpha(\Theta_0)(\Theta_0 - \Theta_{\mathrm{ref}}) + \tfrac{1}{3} e_{\mathrm{pc}}\,(f_s(\Theta) - f_s(\Theta_0))]\,\mathbf{1} \tag{22}$$

where e_{pc} is the volumetric variation due to phase change. Usually, this consists of a volumetric contraction referred to as phase change shrinkage ($e_{\mathrm{pc}} < 0$).

Finally, the thermal term of the free energy $T = \hat{T}(\Theta)$ must be extended to account for the thermal effects of the phase change. In this work, it will take the form

$$T = \hat{T}(\Theta) = \int_{\Theta_0}^{\Theta} \hat{T}_\Theta(\bar{\Theta})\,\mathrm{d}\bar{\Theta} = -\int_{\Theta_0}^{\Theta} \mathrm{d}\bar{\Theta} \int_{\Theta_0}^{\bar{\Theta}} \left[C_0(\hat{\Theta}) + L_\Theta(\hat{\Theta}) \right] \frac{\mathrm{d}\hat{\Theta}}{\hat{\Theta}} \tag{23}$$

where $L = L(\Theta)$ is the latent heat function. It is possible to define the latent heat function in terms of the solid fraction as $L = \mathscr{L} f_s(\Theta)$, with $\mathscr{L}$ constant, but there are other possibilities. Now the entropy will read

$$S = -\partial_\Theta \hat{\Psi} = \int_{\Theta_0}^{\Theta} [C_0(\hat{\Theta}) + L_\Theta(\hat{\Theta})] \frac{\mathrm{d}\hat{\Theta}}{\hat{\Theta}} - \partial_\Theta \hat{W} - \partial_\Theta \hat{H} \tag{24}$$

and the energy balance equation in terms of the temperature, Eq. (13), may be finally rewritten as

$$C_s \dot{\Theta} + \dot{L} = -\nabla \cdot \mathbf{q} + R + \mathscr{D}_{\text{int}} - \mathscr{H}_{\text{ep}} \tag{25}$$

where the heat capacity retains its definition as $C_s = C_0(\Theta) - \Theta \partial^2_{\Theta\Theta}(\hat{W} + \hat{H})$, that is, it does not include the contribution from the latent heat. It is worthy to remark that for solidification processes the last two terms of equation (25) are usually negligible.

The proposed model for liquid–solid phase change can be easily extended to include multiphase changes. This is necessary for most industrial metal alloys, which present one or more solid–solid phase changes in addition to the liquid–solid phase change.

2.4. Thermo-mechanical contact model

In this work, mechanical contact has been modelled using a penalty regularization technique. Frictional contact has been assumed. The interested reader is addressed to [2, 4, 5] for further details.

A thermal contact model at the contact interface is considered, taking into account heat conduction flux through the contact surface, heat generation due to frictional dissipation and heat convection between the interacting bodies when they separate one from each other due to a shrinkage process taking place during solidification [5].

Heat conduction through the contact surface between the solidifying part and the mould has been assumed to be a function of the normal contact pressure, the mean gas temperature and the thermal gap [6, 7]. The heat convection coefficient is therefore a function of the mechanical gap [8, 9]. For some industrial applications, this provides a crucial link between the thermal and mechanical stages of the simulation, motivating the need for a fully coupled thermo-mechanical model.

2.5. Variational formulation

Using standard procedures, the weak form of the momentum balance and reduced energy equations take the following expressions:

$$\begin{aligned} \langle \boldsymbol{\sigma}, \nabla[\boldsymbol{\eta}_0] \rangle &= \langle \mathbf{B}, \boldsymbol{\eta}_0 \rangle + \langle \bar{\mathbf{t}}, \boldsymbol{\eta}_0 \rangle_{\Gamma_\sigma} + \langle \mathbf{t}, \boldsymbol{\eta}_0 \rangle_{\Gamma_{\text{mc}}} \\ \langle C_s \dot{\Theta} + \dot{L}, \zeta_0 \rangle - \langle \mathbf{q}, \nabla[\zeta_0] \rangle &= \langle R + \mathscr{D}_{\text{int}} - \mathscr{H}_{\text{ep}}, \zeta_0 \rangle - \langle \bar{q}, \zeta_0 \rangle_{\Gamma_q} - \langle q, \zeta_0 \rangle_{\Gamma_{\text{tc}}} \end{aligned} \tag{26}$$

which must hold for any admissible displacement and temperature functions $\boldsymbol{\eta}_0$ and ζ_0, respectively. Here, $\bar{\mathbf{t}}$ and $\mathbf{t}$ are the tractions in boundaries Γ_σ and Γ_{mc} (mechanical contact), respectively, and $\bar{q}$ and q are the normal fluxes in boundaries Γ_q and Γ_{tc} (thermal contact), respectively. We address the reader to [5, 10] for a comprehensive description of the derivation of the weak form for coupled thermomechanical frictional contact problems.

3. TIME INTEGRATION OF THE COUPLED PROBLEM

The numerical solution of the coupled thermomechanical initial boundary value problem involves the transformation of an infinite-dimensional transient system, governed by a system of quasi-linear partial differential equations into a sequence of discrete nonlinear algebraic problems by means of a Galerkin finite element projection and a time marching scheme for the advancement of the primary nodal variables, displacements and temperatures, together with a return mapping algorithm for the advancement of the internal variables.

With regard to the time-marching scheme, different strategies are possible to perform this transformation, but they can be grouped in two categories: *simultaneous* time-stepping algorithms and *staggered* time-stepping algorithms.

Simultaneous time-stepping algorithms solve both the mechanical and the thermal equilibrium equations together, thus advancing all the primary nodal variables of the problem, displacements and temperatures, simultaneously. This invariably leads to large and unsymmetric systems of equations, usually prohibitively expensive to solve. Furthermore, the use of different standard time-stepping algorithms developed for the single uncoupled problems is not straightforward, and it is not possible to take advantage of the different time scales possibly involved in the problem for the mechanical and thermal parts. On the other hand, it is relatively simple to devise unconditionally stable schemes using this approach.

A variant of this approach is to attempt the solution of the resulting equations using a block-iterative solution. This leads to smaller and usually symmetric system of equations to be solved, but then the study of the stability of the algorithms is complicated, as it depends on the tolerances used to assess convergence. The problem of stability in time is then linked to that of convergence within the time step [11].

Staggered time-stepping algorithms are based on the use of an operator split, applied to the coupled system of non-linear ordinary differential equations, and a product formula algorithm, which leads to a scheme in which each one of the subproblems defined by the partition is solved sequentially, within the framework of classical *fractional step methods*. This leads to the partition of the original problem into smaller and typically symmetric (physical) subproblems. Furthermore, the use of different standard time-stepping algorithms developed for the uncoupled subproblems is now straightforward, and it is possible to take advantage of the different time scales involved. Additionally, it is now possible to obtain unconditionally stable schemes using this approach, providing that the operator split preserves the underlying dissipative structure of the original problem [12, 13]. In view of these motivations, in this work the staggered scheme has been preferred. Additional details about the formulation, implementation and stability analysis of the method can be found in [2, 3, 12, 13].

In the classical *isothermal split* the coupled system of equations is partitioned into a mechanical phase at constant temperature, followed by a thermal phase at fixed configuration. The evolution of the internal variables is enforced in both phases. As shown in references [12, 13] the isothermal split does not preserve the contractivity property of the coupled problem of non-linear thermoelasticity, resulting in staggered schemes at best only conditionally stables.

In the alternative *isoentropic split*, introduced in [12, 13], and extended for the consideration of phase change phenomena in [2, 3], the coupled problem is partitioned into a mechanical phase at constant entropy, followed by a thermal phase at fixed configuration, leading to an unconditionally stable staggered scheme. The evolution of the internal variables is enforced in both

phases. An efficient implementation of the split can be done using the temperature as primary variable [2].

However, if the mechanical terms appearing in the time derivative of the entropy (see equations (10b) and (12b)) are negligible, that is, the elastoplastic heating $\mathscr{H}_{\text{ep}} = 0$, then the condition of constant entropy in the isoentropic split conveys the condition of constant temperature and both splits are identical. In particular, under these conditions, the standard isothermal split preserves the dissipative structure of the original coupled problem, and it can be shown to be unconditionally stable. As this is the case in most industrial solidification problems, only this split will be described here in detail. The possibilities are twofold: Scheme (a), where the mechanical phase of the operator split is performed before the thermal phase, and Scheme (b), where the thermal phase is performed before the mechanical phase.

Let us first consider Scheme (a):

(a.i) *Mechanical phase.* Using a Backward Euler (BE) time-stepping algorithm, and noting that the temperature and latent heat remain constant during this phase, the discrete weak form of the momentum balance equation and updated internal variables $\mathbf{G} := (\boldsymbol{\varepsilon}_{\text{v}}, \boldsymbol{\varepsilon}_{\text{p}}, \xi)$ in the mechanical phase, take the form

$$\begin{aligned} \langle \tilde{\boldsymbol{\sigma}}_{n+1}, \nabla[\boldsymbol{\eta}_0] \rangle &= \langle \mathbf{B}, \boldsymbol{\eta}_0 \rangle + \langle \bar{\mathbf{t}}_{n+1}, \boldsymbol{\eta}_0 \rangle_{\Gamma_\sigma} + \langle \mathbf{t}_{n+1}, \boldsymbol{\eta}_0 \rangle_{\Gamma_{\text{mc}}} \\ \tilde{\mathbf{G}}_{n+1} &= \mathbf{G}_n + \Delta \tilde{\mathbf{G}}_{n+1} \end{aligned} \tag{27}$$

(a.ii) *Thermal phase.* Using a BE scheme the discrete weak form of the energy balance equation and updated internal variables in the thermal phase take the form

$$\begin{aligned} &\frac{1}{\Delta t} \langle C_{sn+1}(\Theta_{n+1} - \Theta_n) + L_{n+1} - L_n, \zeta_0 \rangle - \langle \mathbf{q}_{n+1}, \nabla[\zeta_0] \rangle \\ &\quad = \langle R_{n+1} + (\mathscr{D}_{\text{int}})_{n+1}, \zeta_0 \rangle - \langle \bar{q}_{n+1}, \zeta_0 \rangle_{\Gamma_q} - \langle q_{n+1}, \zeta_0 \rangle_{\Gamma_{\text{tc}}} \\ &\quad \mathbf{G}_{n+1} = \mathbf{G}_n + \Delta \mathbf{G}_{n+1} \end{aligned} \tag{28}$$

For the simulation of solidification processes and other thermally driven coupled problems (that is, situations where the variation of temperature activates the mechanical part of the problem), it is advantageous to reverse the order of the operator split, and consider Scheme (b), where the thermal phase of the operator split is performed before the mechanical phase:

(b.i) *Thermal phase.* Using a BE scheme the discrete weak form of the energy balance equation and updated internal variables in the thermal phase take the form

$$\begin{aligned} &\frac{1}{\Delta t} \langle C_{sn+1}(\Theta_{n+1} - \Theta_n) + L_{n+1} - L_n, \zeta_0 \rangle - \langle \mathbf{q}_{n+1}, \nabla[\zeta_0] \rangle \\ &\quad = \langle R_{n+1} + (\tilde{\mathscr{D}}_{\text{int}})_{n+1}, \zeta_0 \rangle - \langle \bar{q}_{n+1}, \zeta_0 \rangle_{\Gamma_q} - \langle \tilde{q}_{n+1}, \zeta_0 \rangle_{\Gamma_{\text{tc}}} \\ &\quad \tilde{\mathbf{G}}_{n+1} = \mathbf{G}_n + \Delta \tilde{\mathbf{G}}_{n+1} \end{aligned} \tag{29}$$

(b.ii) *Mechanical phase.* Using a BE time-stepping algorithm, the discrete weak form of the momentum balance equation and updated internal variables $\mathbf{G}$ in the mechanical phase take the form

$$\begin{aligned} \langle \boldsymbol{\sigma}_{n+1}, \nabla[\boldsymbol{\eta}_0] \rangle &= \langle \mathbf{B}, \boldsymbol{\eta}_0 \rangle + \langle \bar{\mathbf{t}}_{n+1}, \boldsymbol{\eta}_0 \rangle_{\Gamma_\sigma} + \langle \mathbf{t}_{n+1}, \boldsymbol{\eta}_0 \rangle_{\Gamma_{\text{mc}}} \\ \mathbf{G}_{n+1} &= \mathbf{G}_n + \Delta \mathbf{G}_{n+1} \end{aligned} \tag{30}$$

Results obtained with Scheme (b) are not the same as those obtained with Scheme (a), but the difference between them is of the order of the size of the time step, $\mathcal{O}(\Delta t)$, which is the order of the error of this type of operator splits. Note that in Scheme (b) the update of the internal variables $\tilde{\mathbf{G}}_{n+1}$ during the thermal phase is only necessary for the evaluation of the term $(\tilde{\mathscr{D}}_{\text{int}})_{n+1}$. In the simulation of solidification processes this term is usually negligible, and therefore this first update of the internal variables can be avoided. This is equivalent to performing an explicit update of the form $(\tilde{\mathscr{D}}_{\text{int}})_{n+1} = (\mathscr{D}_{\text{int}})_n$ and it results in an evident saving in computational cost.

4. NUMERICAL SIMULATIONS

The formulation presented in the previous sections is demonstrated in the following selected numerical simulations. First, an assessment of the constitutive model is presented to establish qualitatively its validity. Then test industrial applications are presented and compared with available experimental data. Finally, a large-size industrial analysis is performed and selected numerical results are shown.

The computations are performed with the finite element code COMET (COupled MEchanical and Thermal analysis) developed by the authors. In all the following numerical simulations the Newton–Raphson method, combined with a line search optimization technique, was used to solve the non-linear equations arising from the spatial and temporal discretization of the weak form of the momemtum and energy balance equations. Convergence of the incremental (in time)—iterative procedure was monitored by requiring a tolerance of 0·1 per cent in the residual-based error norm.

4.1. Assessment of the constitutive model

The overall behaviour of the proposed thermo-(visco)elastic-(visco)plastic model is illustrated here through the numerical simulation of a simple uniaxial tension test. The test is performed at a imposed strain rate of 10^{-4} s^{-1}, sustained from $t = 0$ s to $t = 250$ s. Figure 2 shows the stress response of the model at different temperatures (20, 500, 1000 and 1200°C). The transition between the solid and liquid phases occurs between 1145 and 1155°C, so that the curve at 1200°C corresponds to the purely visco-elastic liquid behaviour, including the total stress unloading when the strain-rate vanishes. For lower temperatures, the dependency of the elastic moduli on the temperature is clearly observed. Also, the effect of visco-plasticity during loading, and the later drop of stress down to the (temperature-dependent) yield stress can be clearly observed in the figure.

4.2. Cylindrical aluminium solidification test

This example, taken from [14], is concerned with the solidification process of a cylindrical aluminium specimen in a steel mould. The geometry is depicted in Figure 3. Assumed starting conditions in the numerical simulation of the solidification process are given by a completely filled mould with aluminium in liquid state at a uniform temperature of 670°C. The initial temperature of the mould is 200°C. Only gravitational forces act on the part and mould. The material properties for the aluminium have been assumed to be temperature-dependent, while constant material properties have been assumed for the steel mould. Geometrical and material data can be found in the above reference. A gap-dependent convection–radiation coefficient between the aluminium and the steel

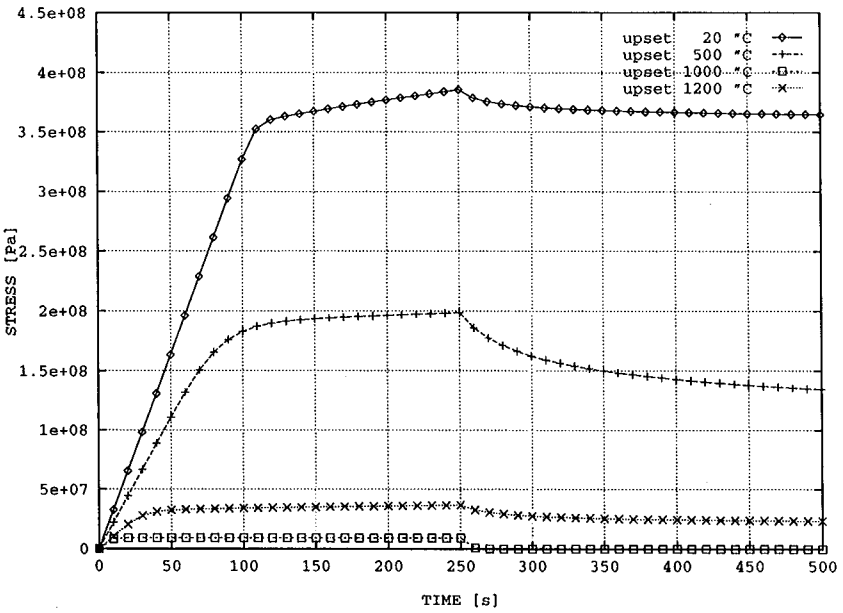

Figure 2. Stress response at different temperatures

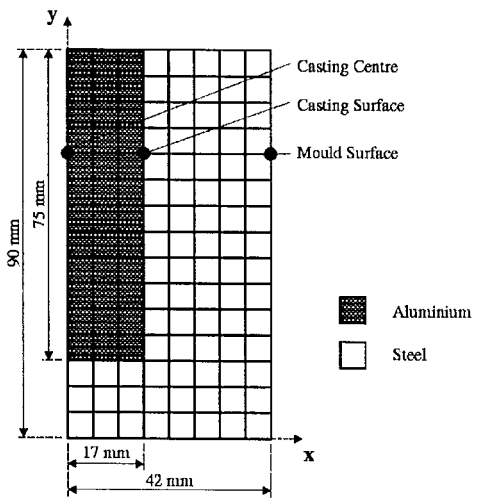

Figure 3. Cylindrical aluminium solidification test. Geometry

mould has been assumed. It takes the form $h(g_n) = k_a/(g_n + k_a/h_o)$, where k_a is the air conductivity, h_o is the convection—radiation coefficient for the two surfaces in contact and g_n is the normal gap.

Spatial discretization of the casting cylinder and the mould has been done using a finite element mesh consisting of 848 axisymmetric 3-noded triangles. Numerical simulation was done up to 90 s. of the solidification test using a time step of 1 s.

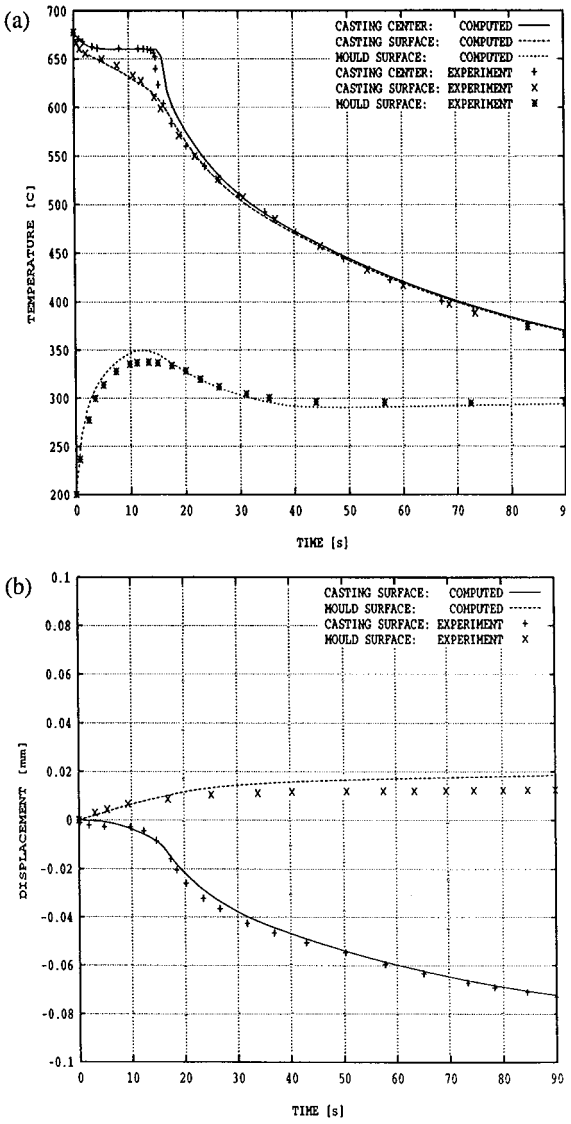

Figure 4. Cylindrical aluminium solidification test: (a) temperature evolution at the casting centre, casting surface and mould surface; (b) radial displacement evolution at the casting and mould surfaces

Figure 4(a) shows the temperature evolution at the casting centre, casting surface and mould surface for an intermediate section. A typical temperature plateau due to the release of latent heat during solidification can be observed for the casting centre point of this section up to 15 s approximately. Figure 4(b) shows the evolution of the radial displacements at the casting and mould surfaces for the same intermediate section. The difference between the two curves gives the gap distance evolution at the chosen section. Computed temperature and gap evolutions compare very well with available experimental results.

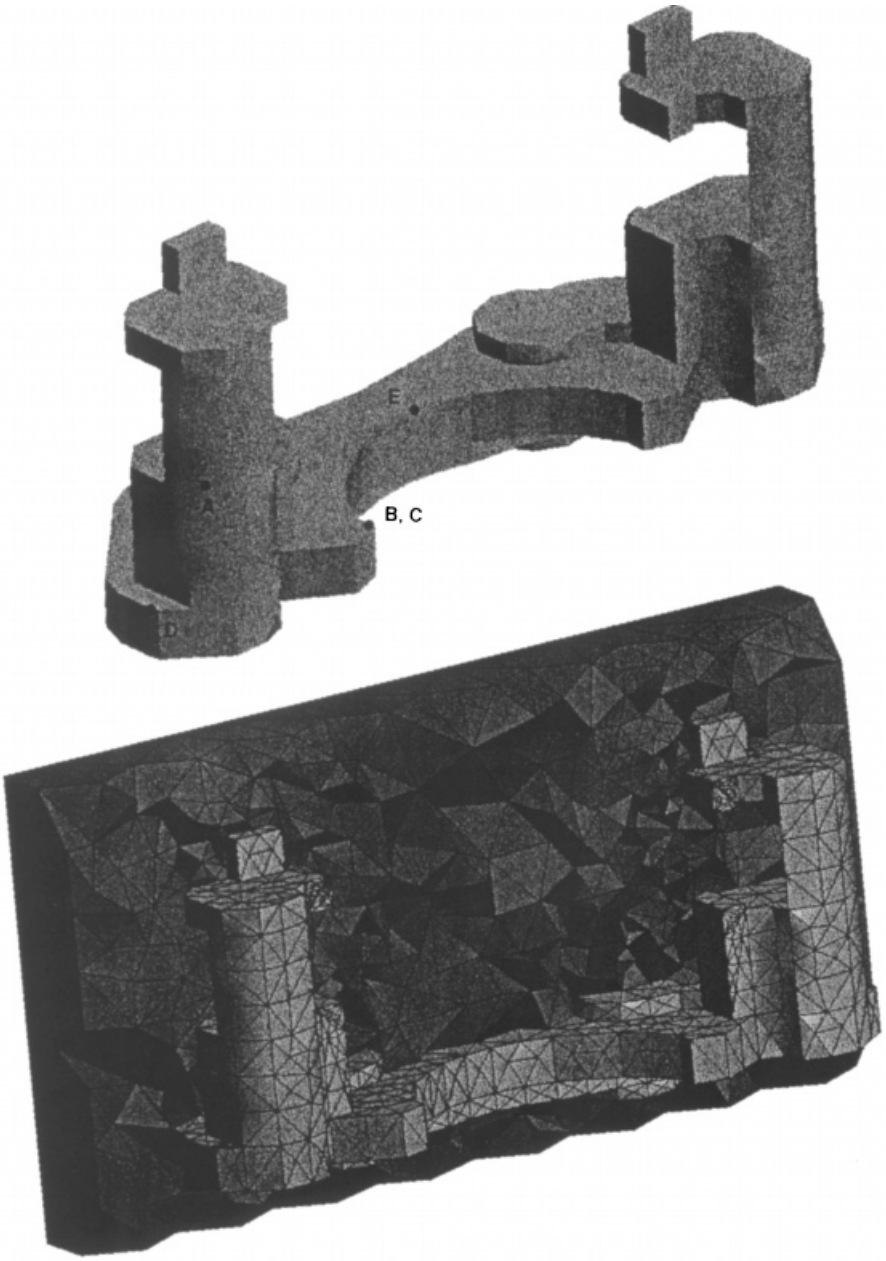

Figure 5. Solidification of a brake component. Geometry and finite element mesh

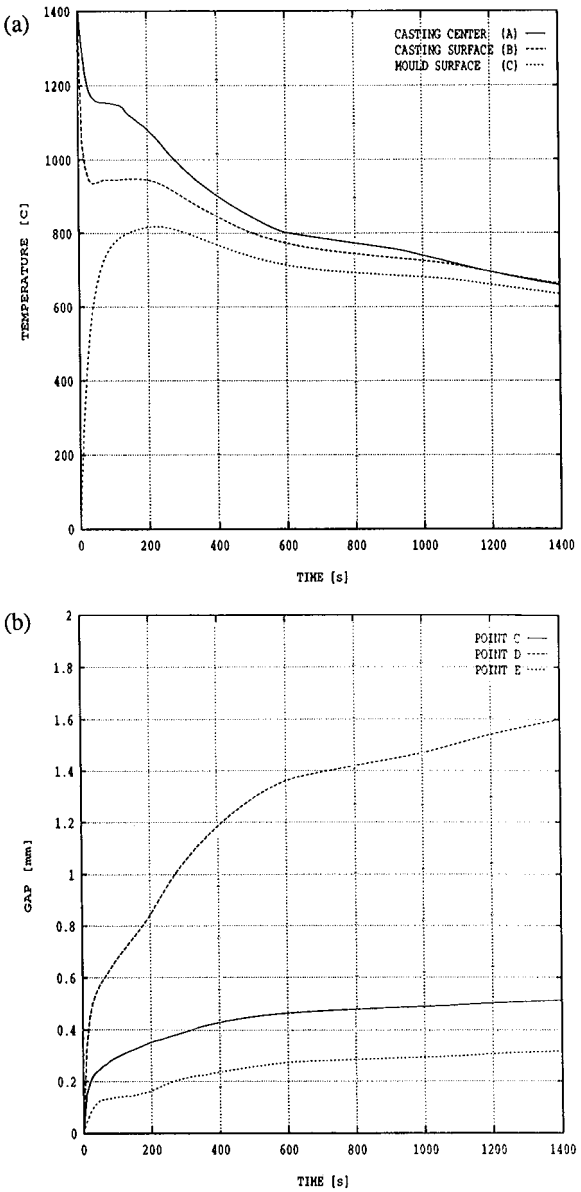

Figure 6. Solidification of a brake component: (a) temperature evolution at the casting centre A, casting surface B and mould surface C; (b) gap evolution at points C, D and E

4.3. Solidification of a brake component

This last example deals with the numerical simulation of the solidification process of an industrial part, in this case, one of the components of the braking system of an automobile. Figure 5 shows a view of the manufactured part (above) and also, a view of the finite element mesh used to

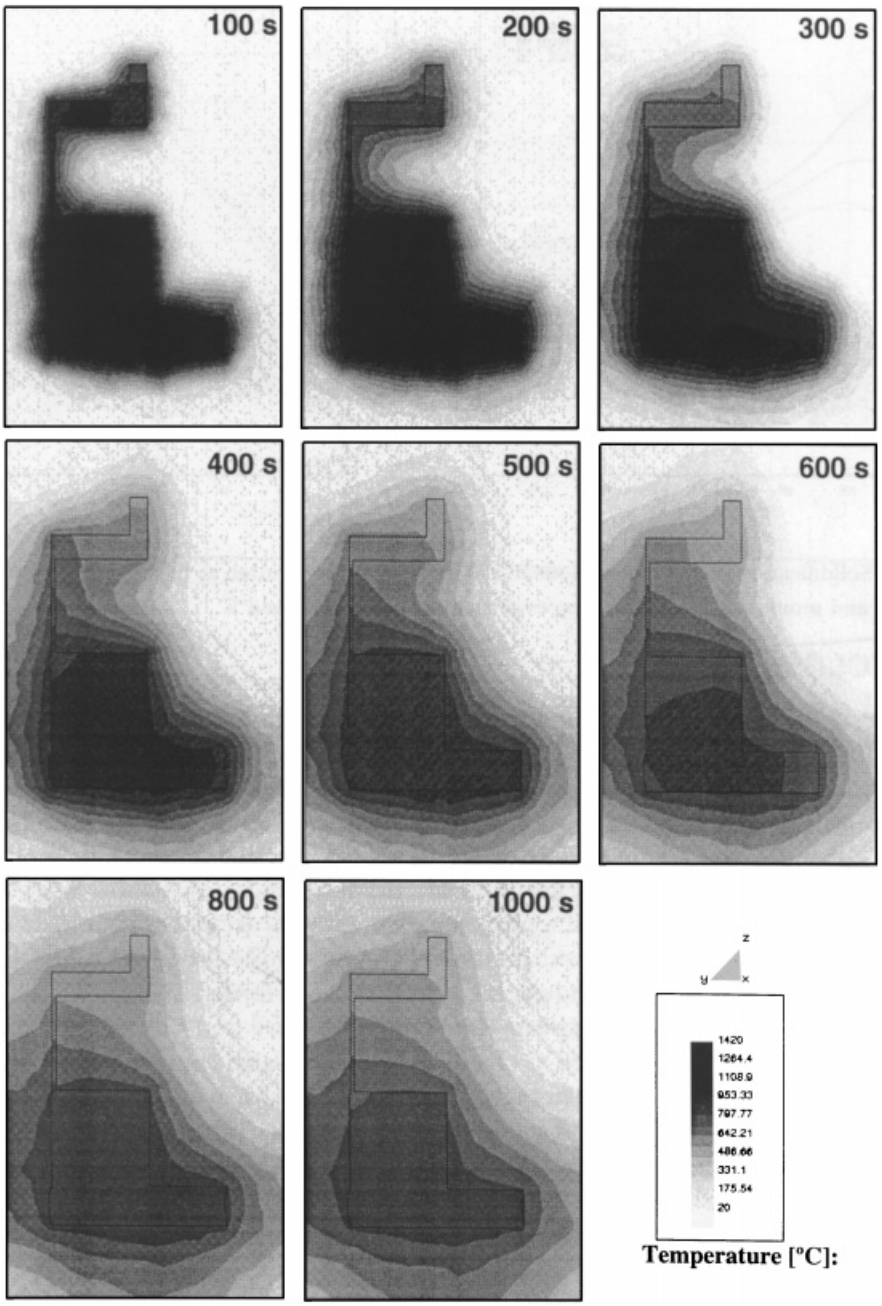

Figure 7. Solidification of a brake component. Temperature evolution on section y–z

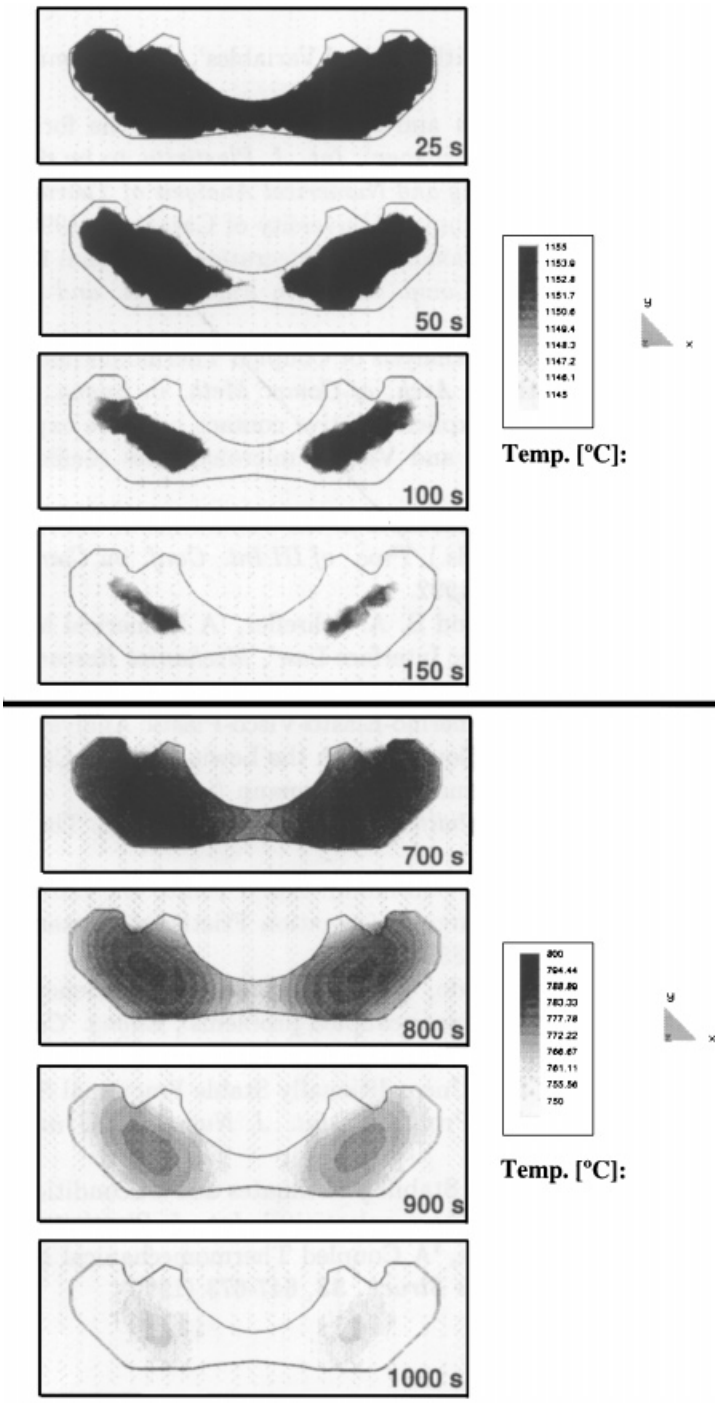

Figure 8. Solidification of a brake component. Evolution of the phase changes on section x–y

discretize the cast iron part and the sand mould (below). The mesh consists of 6500 4-noded tetrahedral elements for the part and 26 650 tetrahedral elements more for the mould. Mechanical, thermal and coupling properties are assumed to be temperature dependent. The cast iron used for the part presents a liquid–solid phase change between 1145 and 1155°C, and a solid–solid phase change between 750 and 800°C. Both phase changes have been accounted for in the simulation. The initial temperature is 1420°C for the part and ambient temperature (20°C) for the mould.

Figure 6(a) shows the temperature evolution at point A, located at the casting centre, point B, located at the casting surface and point C, located at the mould surface (see Figure 5 for the location of the points). A typical temperature plateau due to the release of latent heat during solidification can be observed for the casting centre point (A) up to 150 s. approximately. The smoother solid–solid phase change can also be observed for this point, between 600 and 950 s approximately. Figure 6(b) shows the evolution of the mechanical gaps that develop between the part and the mould for points C, D and E, as the part contracts due to the temperature drop. It is remarkable that the gap at point D grows quite significantly, reaching an amplitude close to 2 mm.

Figure 7 shows the evolution of the temperature distribution on section y–z (a vertical section). Temperature at the core of the part drops during the first 1000 s of the simulation to about 700°C. The evolution of the two phase changes, given by the temperature evolution at the liquid–solid and solid–solid transition ranges, is shown in Figure 8, for section x–y (a horizontal section). The upper part of the figures shows the evolution of the liquid–solid phase change, which takes place during the first 150 s. The lower part of the figures shows the evolution of the solid–solid phase change, which is much slower, starting about 500 s. and still occurring after 1000 s. In this figure the evolution of the gap between the part and the mould, which increases as the volumetric changes due to the cooling process take place is also shown. No plastic deformations are detectable during the cooling process, but significant residual stresses are computed.

5. CONCLUSIONS

A numerical model for the analysis of coupled thermo-mechanical problems, involving frictional contact and thermal multiphase change phenomena, has been presented. Firstly, the constitutive model proposed for the solid phase was introduced, including elasto-plastic effects and viscous strains to account for temperature-dependent elastic moduli. Secondly, the model was extended to account for the phase change phenomena. The principles of this extension are twofold: (a) to include the strain–stress behaviour in the liquid phase and during the phase change, and (b) to include the thermal effects due to the phase change. The resulting model can be readily used for multiphase change problems, as needed for most industrial applications. Thirdly, thermo-mechanical frictional contact is considered between the solidifying part and the mould. Lastly, the numerical solution of the coupled problem is discussed, and the isothermal split operator is described, as well as its advantages. The model has been succesfully applied to the numerical simulation of industrial solidification processes. Temperature and air gap evolution predicted by the numerical model compare very well with available experimental and numerical results.

ACKNOWLEDGEMENTS

Financial support for this work has been provided by Renault under contract CIMNE/1997/001—Affectation: H5.21.41 with CIMNE. This support is gratefully acknowledged.

REFERENCES

1. Coleman BD. Thermodynamics with internal variables. *Journal of Chemistry and Physics* 1967; **47**:597–613.
2. Agelet de Saracibar C, Cervera M, Chiumenti M. On the formulation of coupled thermoplastic problems with phase-change. *International Journal of Plasticity* 1999; **15**:1–34.
3. Chiumenti M. *Constitutive modelling and numerical analysis of thermo-mechanical phase-change systems*. Ph.D. Thesis, Technical University of Catalonia, 1998.
4. Agelet de Saracibar C. A new frictional time integration algorithm for multi-body large slip frictional contact problems. *Computer Methods in Applied Mechanics and Engineering* 1997; **142**:303–334.
5. Agelet de Saracibar C. Numerical analysis of coupled thermomechanical frictional contact problems. Computational model and applications. *Archives of Computational Methods in Engineering* 1998; **5**:243–301.
6. Song S, Yovanovich MM. Explicit relative contact pressure expression: dependence upon surface roughness parameters and Vickers microhardness coefficients. *AIAA*, 1987; Paper 87-0152.
7. Wriggers P, Miehe C. Recent advances in the simulation of thermomechanical contact processes. In *Proceedings of* III *International Conference on Computational Plasticity* Owen *et al*. DRJ, (eds). Pineridge Press: Swansea, 1992; 325–347.
8. Zavarise G, Wriggers P, Stein E, Schrefler BA. A numerical model for thermomechanical contact based on microscopic interface law. *Mechanics Research Communications* 1992; **19**:173–182.
9. Ransing RS, Lewis RW. A thermo-elasto-visco-plastic analysis for determining air gap and interfacial heat transfer coupled with the Lewis–Ransing correlation for optimal feeding design. In *Proceedings of* VIII *International Conference on Casting*, *Welding and Advanced Solidification Processes* Thomas BG, Beckermann C (eds). The Minerals, Metals & Materials Society: San Diego, 1992; 731–738.
10. Laursen TA, Simo JC. A continuum-based finite element formulation for the implicit solution of multi-body, large deformation frictional contact problems. *International Journal for Numerical Methods in Engineering* 1993; **36**: 3451–3485.
11. Cervera M, Codina R, Galindo M. On the computational efficiency and implementation of block iterative algorithms for nonlinear coupled problems. *Engineering Computations* 1996; **13**:4–30.
12. Armero F, Simo JC. A new unconditionally stable fractional step method for nonlinear coupled thermomechanical problems. *International Journal for Numerical Methods in Engineering* 1992; **35**:737–766.
13. Armero F, Simo JC. A priori stability estimates and unconditionally stable product algorithms for nonlinear coupled thermoplasticity. *International Journal of Plasticity* 1993; **9**:749–782.
14. Celentano D, Oller S, Oñate E. A coupled thermomechanical model for the solidification of cast metals. *International Journal of Solids and Structures* 1996; **33**:647–673.

